Role of nitrogen pressure on structural and optical properties of AlN films synthesized by thermal evaporation

I. A. KHAN*, B. HASSAN, S. A. HUSSAIN, S. PERVAIZ
Department of Physics, Government College University Faisalabad, 38000, Pakistan

Surface properties of AlN films synthesized by thermal evaporator for various nitrogen pressures (NP) are investigated. XRD patterns confirms the synthesis of amorphous and crystalline AlN films. SEM analysis reveals the formation of nanoparticles and nanorods distributed uniformly. Refractive index (*n*) of AlN film synthesized for 300 mtorr NP is found to be 1.83. The E_g of AlN films synthesized for 150, 225, 300, 375 mtorr NP are found to be 3.89, 3.24, 3.93, 3.95 eV respectively. Results reveal that the *n*, transmittance and E_g are associated with film thickness which is increased with increasing NP.

(Received June 9, 2020; accepted August 16, 2021)

Keywords: Thin films, Energy band gap, Thermal evaporator, Nanorods

1. Introduction

In this advance era of nanotechnology, the deposition of aluminium nitride (AlN) films on various substrates has noticeable technological importance in the field of material research. These deposited AlN films have outstanding motivating properties like wide energy band gap (6.2 eV), high electrical resistivity (~ 10^{15} Ω cm), high thermal conductivity (~170 W/mK), high breakdown voltage (~3 MV/cm), high hardness (11-15 GPa) and high thermal stability (~1000 °C). The c-axis oriented AlN films are particularly striking for micro-electromechanical and nano-electromechanical devices [1-5]. Alizadeh et al. have studied the photoelectrochemical behavior of AlInN thin films synthesized by plasma assisted dual source reactive evaporation where they have demonstrated that AlInN thin films showed excellent photoelectrochemical behavior for water splitting. They have also demonstrated that the synthesized Al-rich InAlN films can be the promising photo-anode for hydrogen generation from solar water splitting. Additionally, they pointed out that the shifting of optical absorption edge of AlN films from near-ultraviolet region to far-ultraviolet depends upon decreasing substrate distance [6-8]. Moreover, the AlN films has promising features for the fabrication of devices like ultraviolet photodetectors, light-emitting diodes and laser diodes [9-11]. AlN films are used as thermal interface material for high power LEDs [12]. Therefore, AlN has become the subject of intense investigations due to its attractive properties and high application potential in short wavelength LEDs, semiconductor lasers, and UV photodetectors [9-12]. The acoustic response and piezoelectric coefficients of AlN structures depend mainly on their crystallinity, crystal orientation and reduced surface roughness [13-16]. However, more research is still obligatory to point out the influence of structural parameters like the crystal structure, crystallite size, crystallinity, dislocation density, lattice constant and the coexistence of orientations of AlN film on their functionality and applications. Various deposition techniques have been employed with the determination to grow high quality oriented AlN films like pulsed laser deposition [17], molecular beam epitaxy [18], chemical vapor deposition [19], metal organic chemical vapor deposition [20] and magnetron sputtering [21]. Recently, ZnO, Al_2O_3, Cu_2O and ZnAlO films are deposited on various substrates by employing thermal evaporator which is cost-effective deposition technique. It has the advantages owing to produce species of source material having multifarious energy flexes that are responsible to change the growth orientation, crystal structure, morphology, refractive index and energy band gaps [22, 23]. The thin film materials deposited by the thermal evaporator will be cost-effective and will reduce the market price of the component. In the present work, AlN films are deposited on glass substrates by employing thermal evaporator. The AlN films are deposited for various (150, 225, 300 and 375 mtorr) nitrogen pressures (NP_S) while keeping the other deposition parameters. The deposited AlN films are characterized by X-ray diffraction (XRD), scanning electron microscope (SEM) attached with energy dispersive X-ray spectroscopy (EDX) and UV spectroscopic analysis to study the crystal structure, surface morphology, elemental composition and optical properties. A correlation is developed between the refractive index and energy band gap, crystallite size and dislocation density, size and distribution of nanoparticles, and elemental composition. The aim of this study is to deposit AlN “semiconducting material” films through cheaper route. Probably, the deposited AlN films will be used in ultraviolet photodetectors, light-emitting diodes, laser diodes, solar cell and photovoltaic applications.

2. Experimental details

2.1. Chemical

Aluminium (Al) powder (source material) of purity 99 % and glass substrate (dimensions 1 cm × 1 cm) of analytical grade are purchased. Tungsten boat of analytical grade is used to place the source material for evaporation.

2.2. Deposition of AlN film

Deposition of AlN films deposited on glass substrates at various (150, 225, 300 and 375 mtorr) NP_s is accomplished by cost effective thermal evaporator. A schematic diagram of thermal evaporator used to deposit AlN films on glass substrates is illustrated in figure 1. The detailed information's about the homemade thermal evaporator are found in literature [22, 23]. The source material is placed in tungsten boat whereas the substrate holding plate is located at 3 cm apart from the tungsten boat. AlN films are deposited on glass substrates at various NP whereas the other deposition parameters like temperature of tungsten boat (700ºC), treatment time (4 min) and target to substrate distance (3 cm) remains constant. Clean the deposition chamber, loaded the source and substrate materials at their proper locations, closed and evacuated the vacuum chamber down to the pressure of 10^{-2} mbar with rotary pump. The vacuum chamber is filled with nitrogen gas and deposit AlN films at various NP_s by keeping the other parameters (mentioned above) constant. A thermocouple attached with the power supply is used to monitor the boat temperature while a power supply is used to increase the boat temperature.

The basic mechanism behind the formation of AlN films on glass substrate is as follows: the source material acquires enough energy from boat, results in bond breaking and finally the source material is evaporated. The evaporated Al species travels towards the substrate through nitrogen environment and react with each other to form AlN and condensed on the substrate surface in regular or random arrangement depending on their energy fluxes. We hypothesize that the evaporated Al species are of various energies; (i) the high energy Al species reached on the substrate surface in shorter time, may not react with nitrogen and deposit itself on the substrate surface and (ii) the intermediate energy Al species have enough time to react with nitrogen to form AlN and condensed on the substrate surface amorphously or crystalline depending on their energy fluxes. Interestingly, Al_2O_3 phase is formed during the deposition of AlN film at high temperature. However, the formation of Al_2O_3 phase is due to reaction taking place between the evaporated Al and native oxides produced during deposition process at high temperature. The energy flux of evaporated Al species is decreased with the increase of NPs which decreased the mean free path and hence increased the collision rate between the involved species. Hence, the flux of Al, AlN or Al_2O_3 species reaching the substrate surface is decreased which in turn effect on their crystallinity or amorphous nature. Moreover, the evaporated Al species of lower energy may or may not reached on the substrate surface; when reached, they may diffuse or incorporate into the substrate lattice results in lattice distortion creating point defects and vacancies.

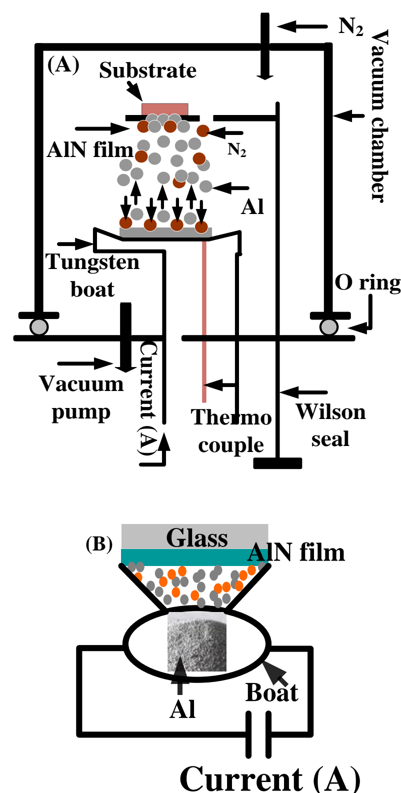

Fig. 1. Schematic diagrams of homemade thermal evaporator used to deposit AlN films (color online)

2.3. Characterizations

The XRD (PAnalytical X'Pert PRO MPD θ-θ X-ray diffractometer, operated at a voltage of 40 kV and a current of 40 mA using a Cu-Kα (λ=1.540598 Å) radiation source) is employed to determine the crystal structure, phase and crystallite size of AlN deposited films at various NPs. The surface morphology and elemental composition of the deposited AlN films have been demonstrated with the help of scanning electron microscopy [FEI NOVA SEM450], provided with energy dispersive X-rays spectroscopy (Oxford INCA X, Act). The optical properties of AlN films are measured by using UV-Visible Spectrophotometer (Genesys-10S).

3. Results and discussion

3.1. Structural analysis

XRD analysis of AlN films deposited at various NP_s on glass substrates by thermal evaporator is used to study their structural information. The average crystallite size (C S) of AlN (101) plane is estimated by using the relation [24, 25].

$$C\ S = \frac{k\lambda}{FWHM\ cos\theta} \quad (1)$$

where k = 0.9 (numerical constant), λ = 1.54 Å (wavelength of incident radiation) and FWHM is the full width at half maximum of the corresponding diffraction plane. The strain (ε) developed in AlN (101) plane is estimated using the relation [26, 27].

$$\varepsilon = \frac{FWHM \cos\theta}{4} \quad (2)$$

The dislocation density (δ), defined as the length of dislocation lines per unit volume of the crystal is estimated by employing the relation [26, 27].

$$\delta = \frac{1}{(C\ S)^2} \quad (3)$$

The weight fraction of AlN (101) and (002) planes is estimated by using the relation [28].

$$V_{[hkl]} = \frac{I_{[hkl]}}{\sum I_{[hkl]}} \quad (4)$$

where I and $V_{[hkl]}$ indicate the peak intensity and weight fraction of AlN plane respectively. The *d-spacing*, lattice parameter (*a*), bond length (*L*) and density of AlN films are calculated by using the relation [29].

$$2d\sin\theta = n\lambda \quad (5)$$

$$d_{(101)} = \left[\frac{4/3(\mathrm{h}^2 + \mathrm{hk} + k^2)}{a^2} + \frac{l^2}{c^2}\right]^{-\frac{1}{2}} \quad (6)$$

$$L = 0.6\ a$$

$$density = \frac{d}{V} \quad (7)$$

where λ, *d*, *a*, *L* and *V* are the wavelength of X-rays, *d*-spacing, lattice constant, bond length and volume of hexagonal AlN crystal respectively.

XRD analysis is employed to study the structural parameters like crystallinity, crystallite size, lattice parameters, strain and dislocation density. Fig. 2 represents the XRD patterns of AlN films deposited on glass substrates at various (150, 225, 300 and 375 mtorr) NP_s by thermal evaporator. The XRD pattern of AlN film deposited at 150 mtorr NP indicates the formation of amorphous nature because no diffraction peak is observed whereas the EDX analysis (discuss later) reveals the existence of Al and N elements. This infers that the Al and N species could not arrange themselves periodically, because at lower NP, the more evaporated Al species having higher energy left away from the active region (along all direction) and hence the remaining lower and insufficient energy flux of involved species could not react with each other as well as arrange themselves periodically. The XRD pattern of AlN film deposited at 225 mtorr NP reveals the development of Al_2O_3 (400), AlN (002) and AlN (101) diffraction peaks. The weak peak intensity shows the weak crystallinity of AlN film. A transformation from amorphous to crystalline AlN film is observed when the pressure is increased from 150 to 225 mtorr of nitrogen gas. The crystallinity of AlN film grows preferentially along (101) orientation is still weak, however, it becomes maximum for 300 mtorr NPs. Moreover, the appearance of Al_2O_3 (400) plane is due to the presence of oxides created during high temperature deposition process and react with the evaporated Al species to form oxides which condensed on the substrate surface. The XRD pattern of AlN film deposited at 300 mtorr NP exhibits the vanishing of Al_2O_3 (400), AlN (002) planes whereas the peak intensity of AlN (101) plane is decreased along with the development of AlN (200) plane. The XRD pattern of AlN film deposited at 375 mtorr NP shows an abrupt structural change in AlN film because all the diffraction planes except AlN (101) plane are vanished. The XRD analysis reveals that the orientation and phase transformation and development of diffraction planes and their crystallinity and nature of AlN films (amorphous or crystalline) are strongly associated with the increase of NP_s. This structural change in AlN films is due to the change in energy flux of involved species with increasing NP_s. Therefore, the change in energy flux of involved species is responsible to change the structural parameters of AlN films. Hence one can control the structural parameters of AlN films by adjusting the working gas pressure. Table 1 shows the detailed change in structural parameters like diffraction angle, FWHM, crystallite size, strains and dislocation densities related to various diffraction planes of AlN films.

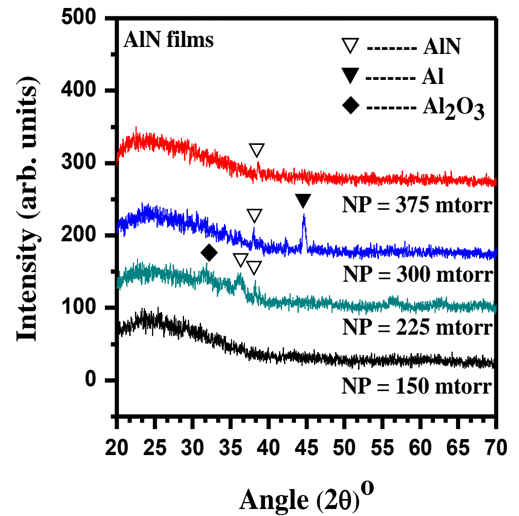

Fig. 2. XRD patterns of AlN films deposited at 150, 225, 300 and 375 mtorr NP_s (color online)

Fig. 3 shows the variation in average C S and peak intensity of AlN (101) plane as a function of increasing NP_s. The average C S of AlN (1 0 1) plane is found to be 66.9, 72.07 and 70.66 nm when the AlN film is deposited at 225, 300 and 375 mtorr NP_s respectively, however, it is maximum at 300 mtorr NP_s which is more favourable for the better growth of AlN film comparatively. It means that the energy flux of involved species available at 300 mtorr NP is suitable to configure them along (101) orientation. On

the other hand, the peak intensity of AlN (101) plane is decreased with the increase of NP_s. It is known that the increase in peak intensity decreases the FWHM of any diffraction peak results in the increases of crystallite size since the C S is inversely proportional to FWHM. In our case, the peak intensity of AlN (101) plane is decreased whereas its average C S is increased with the increase of NP_s and hence there is an inverse relation between the peak intensity and average C S of AlN (101) plane. At higher NP, the decrease in crystallite size is due to the increase in FWHM which is due to the incorporation of impurity atoms or involved evaporated species of smaller energy. The low energy species may not react with the thermally energetic nitrogen species to form AlN phase and may incorporate interstitially results in peak broadening and hence decreases the crystallite size.

Table 1. Change in structural parameters like diffraction angle, FWHM, crystallite size, strains and dislocation densities related to various diffraction planes of AlN films.

NPs (mtorr)	Phases	h k l	$(2\theta)_{ST}$	$(2\theta)_{OB}$	FWHM	C. S. (nm)	Strain	dislocation density × 10^{-3} $(nm)^{-2}$
150	Amorphous film (since no diffraction peak is observed)							
225	Al_2O_3	4 0 0	31.21	31.58	0.86	10.71	0.207	8.68
	AlN	0 0 2	36.03	36.32	0.41	22.73	0.097	1.94
	AlN	1 0 1	38.15	38.29	0.14	66.99	0.033	0.22
300	AlN	1 0 1	38.15	38.11	0.13	72.07	0.031	0.19
	Al	2 0 0	44.72	44.73	0.19	50.43	0.044	0.39
375	AlN	1 0 1	38.15	38.65	0.13	70.66	0.031	0.20

On the other hand, the decrease in peak intensity of AlN (101) with increasing NP indicates the re-crystallization of AlN phase which is due to the decreasing energy of involved species with increasing NP. The diffusion of involved species of smaller energy distorted the lattice of Al or AlN phase creating micro-strains and defects.

Fig. 4 illustrates the variation in δ developed in AlN (101) plane with increasing NP_s. The δ is maximum at lower NP (225 mtorr) which is decreased sharply up to 300 mtorr NP, after that it starts to increase slowly at higher NP. It means that the change in δ developed in AlN (101) plane is associated with the increase of NP_s. This change in δ in AlN (101) plane is responsible to create defects and micro-strains. The calculated value of lattice parameters (a, c) are found to be a = 3.0909 Å and c = 4.9518 Å. The calculated values of lattice parameters "a/c" are higher/smaller than their standard values, thereby indicating the elongation/shrinkage in lattice parameters, creating lattice distortion and hence defects, micro-strains and residual stresses. The elongation/shrinkage in lattice parameters is due to the incorporation of impurity species interstitially and temperature gradient developed at the substrate surface during deposition process. The bond length "L" and density "δ" of AlN film are found to be 1.88 Å and 5.28 $(nm)^{-2}$ respectively. The values of weight fraction of AlN (101) plane is increased from 0.35, 0.39 and 1 with increasing NP_s. This change in weight fraction depends on the nucleation and growth of AlN film along various orientations. The XRD results of AlN films exhibit that the deposition of amorphous and crystalline AlN film, the change in structural parameters and the change in lattice parameters of AlN films with increasing NP_s. Table 1 shows that the diffraction AlN (101) plane is shifted upward or downward with the increase of NPs. It is well known that the up and down shifting of any diffraction plane indicates the presence of residual stresses, if the diffraction peak is shifted upward, this infers that a compressive stress is present. On the other hand, if the diffraction peak is shifted downward, this infers that a tensile stress is present. Table 1reveals that the presence of compressive or tensile stress in the deposited AlN film is strongly associated with the increase of NPs.

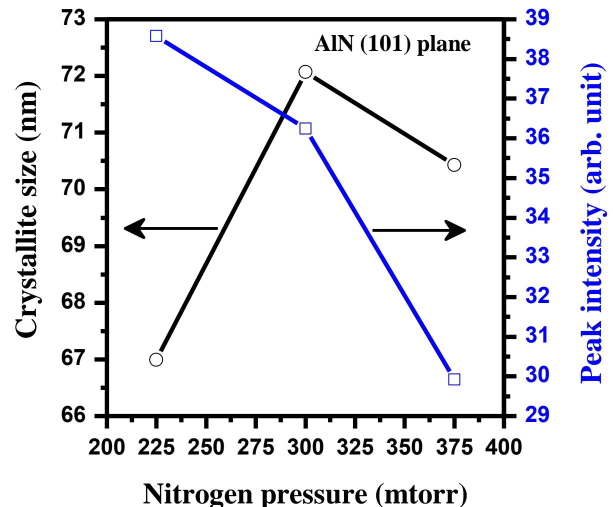

Fig. 3. Variation of average C S and peak intensity of AlN (101) plane with increasing NP_s (color online)

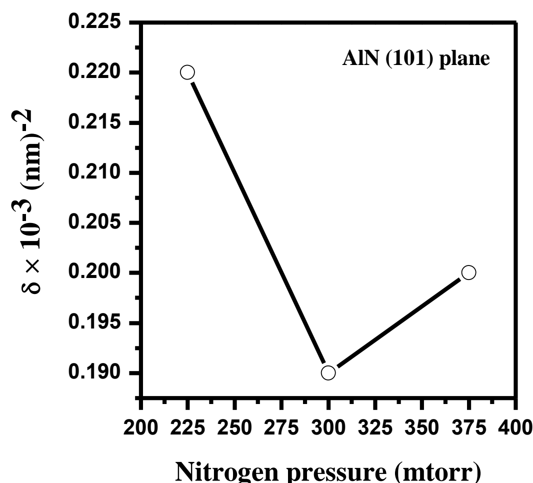

Fig. 4. Variation of δ developed in AlN (101) plane with increasing NP_s

3.2. SEM analysis

The surface morphology of AlN films deposited at various (150, 225, 300 and 375 mtorr) NP_s by thermal evaporator is investigated by SEM analysis. Fig. 5-A demonstartes the formation of rounded nano-particles (size ranged from 110-120 nm) of AlN film deposited at 150 mtorr NP.

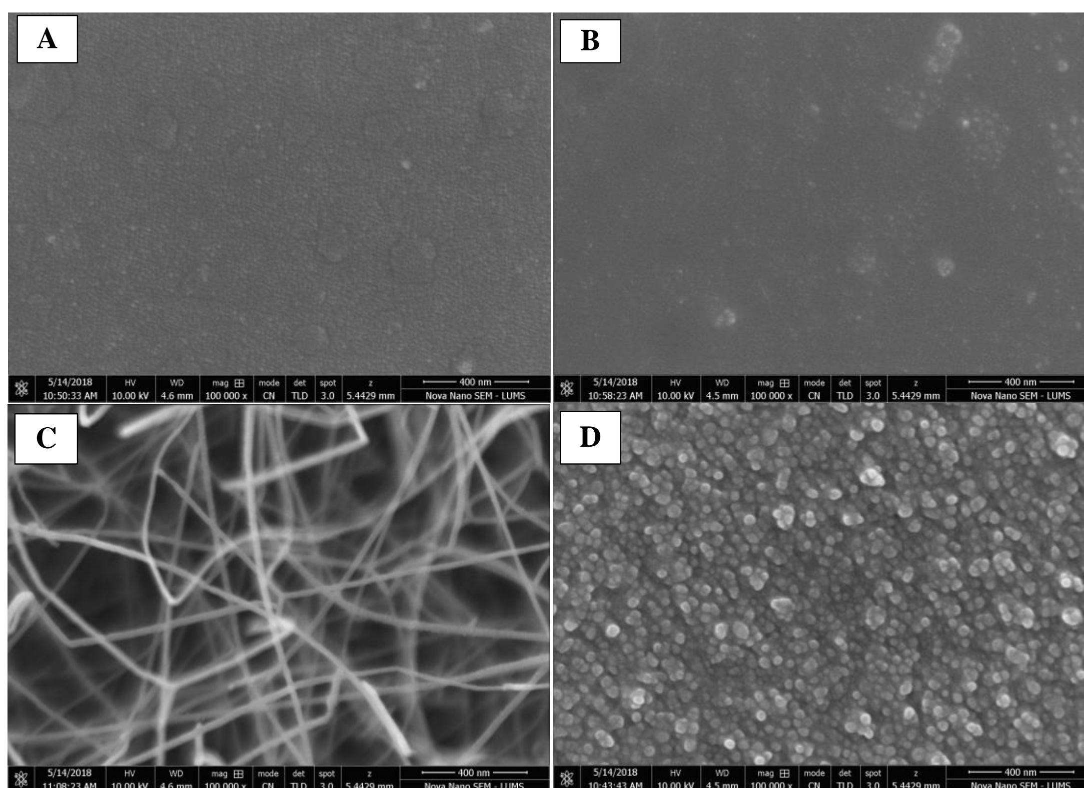

Fig. 5. SEM microstructures of AlN films deposited at (A) 150, (B) 225, (c) 300 and (D) 375 mtorr NP_s

The distribution of rounded nano-particles is uniform whereas the outlook appearence shows the formation of smooth surface, however, the colonies of closely packed nano-particles are also observed. The colonies of nano-particles are embaded into the uniform distribution of other nano-particles. These colonies are seperated from the other uniformly distributed nano-particles through their boundaries. Fig. 5-B exhibits the formation of again rounded nano-particles (size ranged from 60-120 nm) of AlN film deposited for 225 mtorr NP. The distribution of nano-particles is uniform whereas the outlook appearence shows the formation of smooth surface. The clouds of nano-partilces with shiny appearence are also observed. Fig. 5-C exhibits the formation of nano-rods (diameters ranged from 110-330 nm) of AlN film deposited at 300 mtorr NP. These nano-rods make a complicated network covering the entire scanned area uniformly. However, the appearence of dark regions where no nano-rods are observed makes the surface rough. It seems that the nano-rods are stacked one above the others forming complicated layers of nano-rods of AlN film.

Fig. 5-D reveals the formation of rounded nano-particles and their clusters. The diameter of rounded nano-particles distributed uniformly is ranged from 111-555 nm.

The outlook appearence shows the formation of rough surface which is due to the formation of dark and bright humps.

The clusters consisting of nano-particles are seemed to grow vertically upwards. From the SEM analysis, the formation of rounded nano-particles, shape, size and distribution of nano-partoicles, surface roughness and the formation of clusters are associated with the increase of NP_s. It is concluded that the surface morphologies of AlN films is strongly associated with the increase of NP_s that is why the formation of nano-rods is observed only at 300 mtorr NP. Moreover, the surface morphology of AlN films deposited at 150 and 225 mtorr NP_s are smooth whereas the surface morphologies of AlN films deposited at 300 and 375 mtorr NP_s are rough in nature comparatively.

3.3. Quantitative analysis

The quantitative analysis of AlN films deposited for various NP_s by thermal evaporator is examined through EDX technique. The EDX image of AlN film deposited at 300 mtorr NPs is shown in Fig. 6. The EDX image shows the presence of Al, N and O along with other peaks related to glass substrate. The presence of Al and N confirms the deposition of AlN films. The oxygen in the deposited AlN films is formed during the deposition process at high temperature. These oxides are so-called native oxides which play an important role to change the film surface properties.

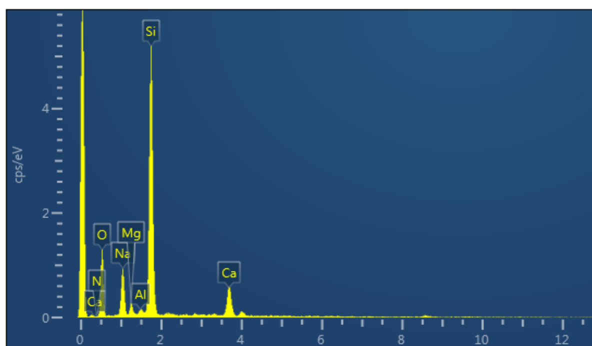

Fig. 6. EDX spectrum of AlN film deposited at 300 mtorr NP (color online)

Table 2 shows the variation of Al, N and O (at. %) contents with increasing NPs. The Al content is increased up to 300 mtorr NPs, after that it is decreased. The change in N contents is strongly associated with the increase of NP_s. however, it is found that the N and Al contents are maximum at 225 and 300 mtorr NP_s respectively. In short, the variation of Al, N and O plays a vital role to change the film surface properties.

Table 2. Shows the variation of Al, N and O (at. %) contents with increasing NPs

NPs (mtorr)	Elemental composition (at. %)		
	Al	N	O
150	0.53	3.5	0.4
225	0.67	7.14	0.6
300	0.69	5.63	0.4
375	0.50	6.65	0.3

3.4. Optical analysis

AlN film is transparent in visible region and hence the optical parameters like transmittance film thickness, refractive index and optical energy band gap of AlN films deposited on glass substrates at various (150, 225, 300 and 375 mtorr) NP_s by thermal evaporator; are determined by using UV spectrometer. Fig. 7 illustrates the transmittance of AlN films deposited at various NP_s. The transmittance of AlN films at $\lambda = 632$ nm are found to be 99.33, 93.05, 88.33 and 86.76 deposited for 150, 225, 300 and 375 mtorr NP respectively. This indicates that the deposited AlN film is highly transparent, however, the transparency of AlN films is decreased with the increase of NPs. We classified AlN films into two domains: (i) amorphous (AlN film deposited for 150 mtorr NP), (ii) weakly crystalline (AlN films deposited for 225, 300 and 375 mtorr NP). The weakly crystalline AlN film deposited for 225 mtorr NP contains Al_2O_3 phase. The absorption edges of amorphous AlN film, weakly crystalline AlN films are found to 324, 328 and 384 nm respectively. It is obvious that a blue and red shift in the absorption edge of amorphous AlN and AlN film having crystalline Al_2O_3 phase is associated with the increase of NPs as well as structural nature of deposited AlN films. This shows that the alteration of film nature (from amorphous to crystalline) and the presence Al_2O_3 phase in crystalline AlN film are responsible for the absorption edge shifting.

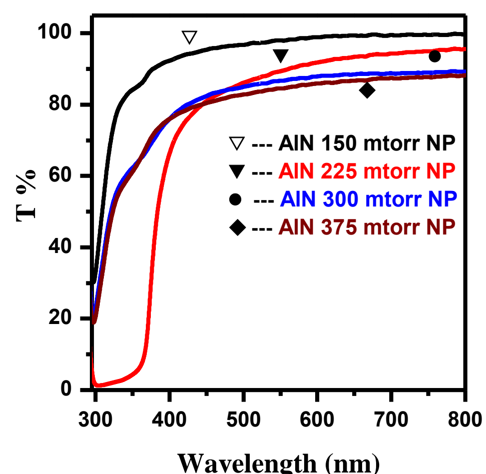

Fig. 7. Variation in transmittance of AlN films deposited at 150, 225, 300, 375 mtorr NPs (color online)

However, the native oxide formed during the deposition process plays an important role to shift the absorption edge of AlN film. The native oxides may or may not react with Al to form Al_2O_3 phase depending on their energy's fluxes. The presence of randomly native oxides (non-reactive) and Al_2O_3 phase (reactive oxides) in AlN film causes to blue and red shifts in absorption edge of AlN films. The decreasing transparency of AlN films with increasing NPs indicates that the film thickness is increased (discuss later). It is known that the surface roughness is associated with the film thickness, so increase in film thickness increases the surface roughness and an increase in surface roughness scatters more the incident light which can contribute to reduce the transparency of AlN films and hence increase the refractive index [30, 31]. Moreover, the thicker film becomes more defective due to the incorporation/diffusion of species of smaller energies into Al or AlN lattice and hence the film becomes denser results in the decrease in film transparency. Now we estimate the refractive index (*n*) of AlN films deposited for various NPs by employing the following relation [30, 31].

$$n = [N + (N^2 - S^2)^{0.5}]^{0.5}$$

where

$$N = 2S\,\frac{T_M - T_m}{T_M T_m} + \frac{S^2 + 1}{2}$$

T_M and Tm denote the transmission values (maximum and minima) at the wavelengths while S is the refractive index of glass. The thickness *(d)* of AlN film is estimated by employing the relation [30, 31]:

$$d = \frac{\lambda_1 \lambda_2}{2(\lambda_1 n_2 - \lambda_2 n_1)}$$

The n_1 and n_2 are the refractive indices at two adjacent maxima (or minima) at the corresponding wavelengths λ_1 and λ_2.

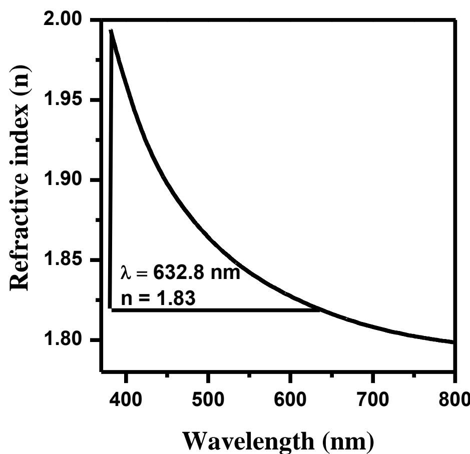

Fig. 8. Variation of refractive index of AlN film deposited at 300 mtorr NP

Fig. 8 shows the variation of refractive index of AlN film deposited for 300 mtorr NP as function of wavelength. The refractive index is decreased with the increase of wavelength. The value of refractive index of AlN film at λ = 632.8 nm is found to 1.83 which is agreed well with the reported values [31, 32]. Fig. 9 (a, b, c) exhibits the variation of thickness and refractive index of AlN films with increasing NPs and the refractive index with increasing film thickness respectively. It is obvious that the film thickness and refractive index of AlN film is increased with the increase of NPs which shows that there is a direct relation between the film thickness and refractive index as shown in Fig. 9_C. In actual practice, the film thickness should be decreased with the increase of NPs, but in the present case, the substrate is placed close to (at 3 cm distance) the source material and the evaporated species of Al may or may react with nitrogen species depending on their energies. If the Al and N species are of enough energy, they react with each other forming AlN and condense on the substrate surface in the form of layer. If the Al and N species do not have enough energies, they may not react with each other but have the aptitude to condense onto the substrate surface with or without constituting crystalline patterns (periodic arrangement) or amorphous nature (random arrangement). It is known that the energy flux reached on the substrate surface is associated with the collisional rate of involved species during their travelling and nucleation towards the substrate surface, more the collisional rate, smaller will be the energies of involved species reached on the substrate surface. It is obvious that the collisional rate between the involved species is increased with the increase NPs. It means that the total amount of involved species having smaller energies is increased with the increase of NPs. These low energy species could not react with each other but have the tendency to condense on the substrate surface, may diffuse into the Al or AlN lattice or condense amorphously results in the increase of film thickness. Fig. 9_B shows the variation of refractive index of AlN films with increasing NPs. The refractive index of AlN films, measured at λ = 632.8 nm, is increased with the increase of NPs. There is a direct relation between the refractive index and film thickness of AlN films deposited by thermal evaporator at various NPs. It means that the refractive index of AlN films is increased with the increase of film thickness whereas the thickness of AlN films is increased with the increase of NPs. The increase in film thickness shows that the film becomes denser with increasing NPs which decreases the transparency of AlN films (Fig… 7). Therefore, it is concluded that there is a direct relation between the film thickness and refractive index while an inverse relation between film thickness/refractive index with the transparency of AlN film.

For the determination of optical energy band gap of AlN films, we used Tauc's relation [33].

$$\alpha h v = A(hv - E_g)^{0.5}$$

where *h* is the photon energy, *A* is a constant and *Eg* is the optical energy band gap. The optical energy band gap of

AlN films is determined by extrapolating the linear portion of the plot of $(\alpha h\nu)^2$ verses $h\nu$ such that the point where $(\alpha h\nu)^2$ is equal to zero gives the value of optical energy band gap of AlN films. Fig. 10 shows the plot of $(\alpha h\nu)^2$ verses $h\nu$ of AlN films deposited at various NPs. The values of optical energy band gap of AlN films deposited at 150, 225, 300 and 375 mtorr NPs are found to be 3.89, 3.24, 3.93 and 3.95 eV respectively. It is obvious that the optical energy band gap of AlN is increased with the increase of NPs except the AlN film deposited at 225 mtorr NPs. This drastically decrease in the value of optical energy band gap of AlN film is due to the presence of oxygen interstitially and the nucleation of Al_2O_3 phase showing weak crystallinity. It means that the presence of oxygen in Al or AlN lattice interstitially and the nucleation of Al_2O_3 phase is responsible to decrease the optical energy band gap of AlN film significantly. Results show that the calculated values of optical energy band gap of AlN films, varied from 3.89, 3.24, 3.93, 3.95 eV, are smaller than the reported values 4.10, 4.15 eV and 5.9 - 6.2 eV [2, 34-37]. It has pointed out that the values of optical energy band gap of sputtered AlN films were found to be in the ranged from 3.8 to 5.9 eV [38]. In our case, the significantly lower values of energy band gap of AlN films are associated with the structural change like lattice parameters, d-spacing, impurities diffusion, micro-strains, vacancies and defects formations as well as morphological changes. The significant decrease in the value of optical energy band gap of AlN film deposited at 225 mtorr NPs is due to the presence of oxygen interstitially and the nucleation of Al_2O_3 phase showing weak crystallinity.

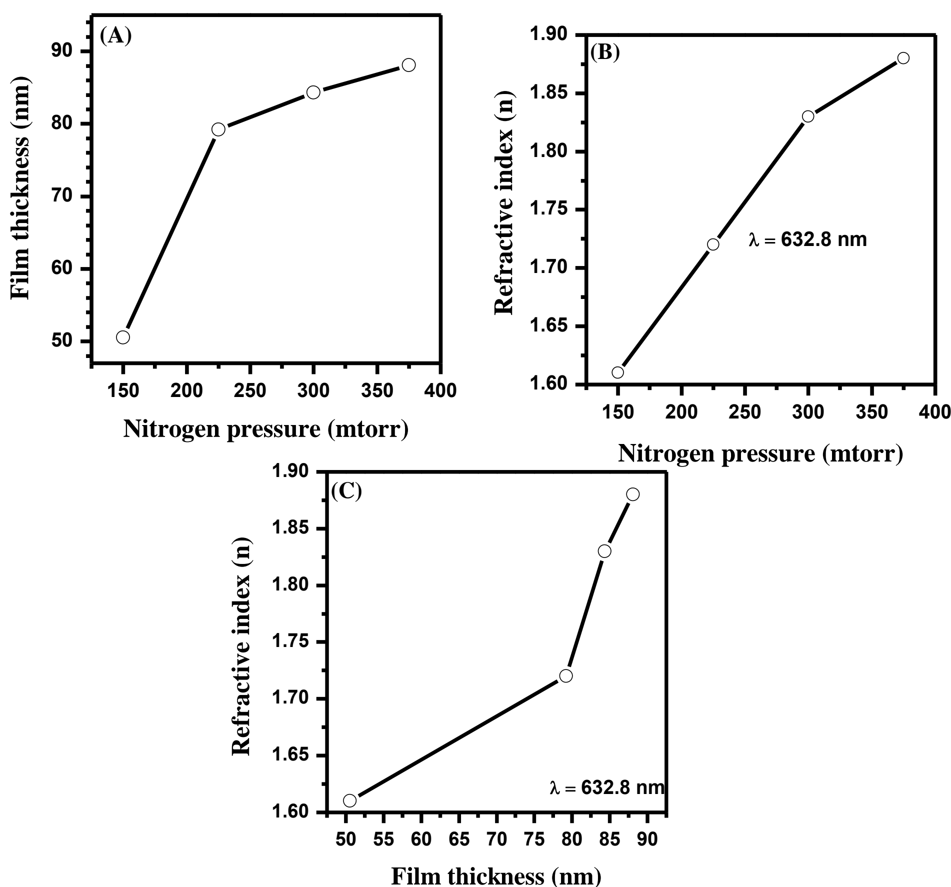

Fig. 9. Variation of (A) film thickness; (B) refractive index of AlN films with increasing NPs and (C) refractive index with increasing film thickness, respectively

The formation of Al_2O_3 phase showing weak crystallinity may be the major reason because Al_2O_3 phase is not present in all other AlN films deposited by thermal evaporator. Therefore, it is concluded that the film thickness and refractive index both are increased with the increase of NPs whereas the transmittance of AlN films decreases with the increase of NPs.

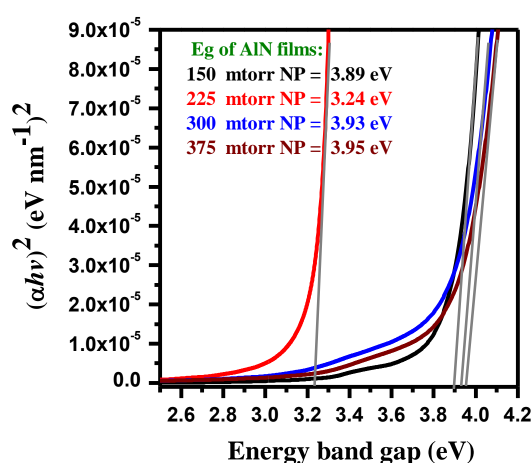

Fig. 10. Variation of energy band gap of AlN films with increasing NPs (color online)

4. Conclusions

AlN films are deposited on glass substrates at various (150, 225, 300 and 375 mtorr) NPs by thermal evaporator. The XRD analysis of AlN films reveals the deposition of amorphous and weakly crystalline AlN films along with the formation of Al_2O_3 phase. The change in structural parameters is associated with the increase of NPs. There is an inverse relation between the crystallite size and peak intensity of AlN (101) plane. SEM analysis confirms the formation of rounded nanoparticles and nano-rods; however, their formation depends on the energy flux of involved species reached on the substrate surface. EDX analysis exhibits the presence of Al, N and O whose contents are changed with increasing NPs. Refractive index of AlN film is found to be 1.83 at λ = 632.8 nm. The refractive index and film thickness are increased with the increase of NPs. These parameters constitute a direct relation between them with increase NPs. The E_g of AlN film deposited at 375 mtorr NP is found to be 3.95 eV. The E_g of AlN films is decreased whereas the film thickness is increased with the increase of NPs. The increase in film thickness leads to decrease the E_g of AlN films. The co-existence of Al_2O_3 and AlN phases plays an important role in the further narrowing in E_g of AlN film. A thicker film shows a higher refractive index owing to its denser and defective nature and hence lower E_g of AlN films, moreover, lower the transparency, higher is the E_g of AlN film. The AlN films show high transparency in visible region may be utilized in solar photovoltaic technology so the achieved AlN films may be the promising materials for applications in microelectronic and optoelectronic devices.

Acknowledgments

The authors would like to thank the Higher Education Commission, Pakistan for proving funds to install thermal evaporator at Thin Films Deposition Lab, Department of Physics, Government College University Faisalabad.

References

[1] B. Abdallah, A. Chala, P. Y. Jouan, M. P. Besland, M. A. Djouadi, Thin Solid Films **515**, 7105 (2007).
[2] C. L. Huang, K. W. Tay, L. Wu, Mater. Lett. **59**, 1012 (2005).
[3] R. Dahal, T. M. Al-Tahtamouni, J. Y. Lin, H. X. Jiang, Appl. Phys. Lett. **91**, 243503 (2007).
[4] C. Duquenne, M.P. Besland, P. Y. Tessier, E. Gautron, Y. Scudeller, D. Averty, J. Phys. D. Appl. Phys. **45**, 015301 (2012).
[5] R. B. Karabalin, M. H. Matheny, X. L. Feng, E. Defa, G. Le-Rhun, C. Marcoux, S. Hentz, P. Andreucci, M. L. Roukes, Appl. Phys. Lett. **95**, 103111 (2009).
[6] M. Alizadeh, V. Ganesh, A. Pandikumar, B. T. Goh, S. Azianty, N. M. Huang, S. A. Rahman, Journal of Alloys and Compounds **670**, 229 (2016).
[7] M. Alizadeh, G. B. Tong, M. S. Mehmood, K. W. Qader, S. A. Rahman, B. Shokri, Solar Energy Materials and Solar Cells **185**, 445 (2018).
[8] M. Alizadeh, B. T. Goh, S. A. Rahman, Metallurgical and Materials Transactions A **48A**, 3461 (2017).
[9] K. Y. Zang, S. J. Chua, L. S. Wang, C. V. Thompson, Phys. Status Solidi C **7**, 2067 (2003).
[10] M. Mosca, J-L. Reverchon, F. Omnes, J.-Y. Duboz, J. Appl. Phys. **95**, 4367 (2004).
[11] S. Arulkumaran, T. Egawa, S. Matsui, H. Ishikawa, Appl. Phys. Lett. **86**, 123503 (2005).
[12] S. Shanmugan, D. Mutharasu, A. H. Haslan, Inter. J. of Elect. & Comp. Sci. Eng. **2(1)**, 296 (2012).
[13] A. Artieda, C. Sandu, P. Muralt, J. Vac. Sci. Technol. A **28**, 390 (2010).
[14] A. E. Wickenden, L. J. Currano, T. Takacs, J. Pulskamp, M. Dubey, S. Hullavarad, R. D. Vispute, Integr. Ferroelectr. **54**, 565 (2003).
[15] T. Kamohara, M. Akiyama, N. Ueno, M. Sakamoto, K. Kano, A. Teshigahara, N. Kawahara, N. Kuwano, Appl. Phys. Lett. **89**, 243507 (2006).
[16] M. Akiyama, T. Kamohara, K. Kano, A. Teshigahara, N. Kawahara, Appl. Phys. Lett. **93**, 021903 (2008).
[17] A. Szekeres, Z. Fogarassy, P. Petrik, E. Vlaikova, A. Cziraki, G. Socol, C. Ristoscu, S. Grigorescu, I. N. Mihailescu, Appl. Surf. Sci. **257**, 5370 (2011).
[18] R. Chandrasekaran, T. D. Moustakas, A. S. Ozcan, K. F. Ludwig, L. Zhou, D. J. Smith, J. Appl. Phys. **108**, 043501 (2010).
[19] A. N. Redkin, A. N. Gruzintsev, Z .I. Makovei, V. I. Tatsii, E. E. Yakimov, Inorg. Mater. **42**, 627 (2006).
[20] C. H. Chiang, K. M. Chen, Y. H. Wu, Y. S. Yeh, W. I. Lee, J. F. Chen, K. L. Lin, Y. L. Hsiao, W. C. Huang, E. Y. Chang, Appl. Surf. Sci. **257**, 2415 (2011).
[21] N. Mutsukura, H. Shinoda, Thin Solid Films **520**, 4237 (2012).
[22] I. A. Khan, M. Noor, A. Rehman, A. Farid, M. A. K. Shahid, M. Shafiq, Eur. Phys. J. Appl. Phys. **72**, 30302 (2015).
[23] I. A. Khan, N. Amna, N. Kanwal, M. Razzaq, A. Farid, N. Amin, U. Ikhlaq, M. Saleem, R. Ahmad,

Mater. Res. Express. **4**, 036402 (2017).
[24] M. García-Méndez, S. Morales-Rodríguez, R. Machorro, W. De, L. Cruz, Rev. Mex. Fis. **54**, 271 (2008).
[25] V. Dumitru, C. Morosanu, V. Sandu, A. Stoica, Thin Solid Films **359**, 17 (2000).
[26] R. Thapa, S. Saha, K.K. Chattopadhyay, Appl. Surf. Sci. **255**, 4536 (2009).
[27] L. F. Jiang, W. Z. Shen, H. Ogawa, Q. X. Guo, J. Appl. Phys. **94**, 5704 (2003).
[28] N. Kumari, A. K. Singh, P.K. Barhai, Int. J. Thin Fil. Sci. Tec. **3**, 43 (2014).
[29] H.-E. Cheng, T.-C. Lin, W.-C. Chen, Thin Solid Films **425**, 85 (2003).
[30] R. Swanepoel, J. Phys. E. **16**, 1214 (1983).
[31] F. Hajakbari, M. M. Larijani, M. Ghoranneviss, M. Aslaninejad, A. Hogabri, Jpn. J. Appl. Phys. **49,** 095802 (2010).
[32] S. Liu, M. Peng, C. Hou, Y. He, M. Li, X. Zheng, Nanoscale Res. Lett. **12**, 279 (2017).
[33] J. Tauc, A. Menth, J. Non. Cryst. Solids. **8-10**, 569 (1972).
[34] H-Y. Joo, H. J. Kim, S. J. Kim, S. Y. Kim, J. Vac. Sci. Technol. A. **17**, 862 (1999).
[35] J. Baek, J. Ma, M. F. Becker, J. W. Keto, D. Kovar, Thin Solid Films **515**, 7096 (2007).
[36] S. Bakalova, A. Szekeres, S. Grigorescu, E. Axente, G. Socol, I. N. Mihailescu, Appl. Phys. A Mater. Sci. Process **85**, 99 (2006).
[37] S. Q. Wang, H. Q. Ye, J. Phys. Condens. Matter. **14**, 9579 (2002).
[38] M. Clement, E. Iborra, J. Sangrador, A. Sanz-Hervás, L. Vergara, M. Aguilar, J. Appl. Phys. **94**, 1495 (2003).

*Corresponding author: ijazahmad@gcuf.edu.pk